

Intratumoral STING agonist reverses immune evasion in PD-(L)1-refractory Merkel cell carcinoma: mechanistic insights from detailed biomarker analyses

Thomas Pulliam ¹, Saumya Jani,¹ Peter H Goff ^{2,3}, Rashmi Bhakuni,¹ Shira Tabachnick-Cherny,¹ Kimberly Smythe ², Brandon W Seaton,² Lisa Tachiki ^{2,4}, Rima Kulikauskas,¹ Candice Church ¹, David M Koelle ^{2,5}, Paul Nghiem ^{1,2}, Shailender Bhatia ^{2,6}

To cite: Pulliam T, Jani S, Goff PH, *et al.* Intratumoral STING agonist reverses immune evasion in PD-(L)1-refractory Merkel cell carcinoma: mechanistic insights from detailed biomarker analyses. *Journal for ImmunoTherapy of Cancer* 2024;**12**:e009803. doi:10.1136/jitc-2024-009803

► Additional supplemental material is published online only. To view, please visit the journal online (<https://doi.org/10.1136/jitc-2024-009803>).

Received 04 June 2024

Accepted 20 September 2024



© Author(s) (or their employer(s)) 2024. Re-use permitted under CC BY-NC. No commercial re-use. See rights and permissions. Published by BMJ.

For numbered affiliations see end of article.

Correspondence to

Dr Shailender Bhatia; sbhatia@uw.edu

ABSTRACT

Background Antibodies blocking programmed death (PD)-1 or its ligand (PD-L1) have revolutionized cancer care, but many patients do not experience durable benefits. Novel treatments to stimulate antitumor immunity are needed in the PD-(L)1 refractory setting. The stimulator of interferon genes (STING) protein, an innate sensor of cytoplasmic DNA, is a promising target with several agonists in development. However, response rates in most recent clinical trials have been low and mechanisms of response remain unclear. We report detailed biomarker analyses in a patient with anti-PD-L1 refractory, Merkel cell polyomavirus (MCPyV)-positive, metastatic Merkel cell carcinoma (MCC) who was treated with an intratumoral (IT) STING agonist (ADU-S100) plus intravenous anti-PD-1 antibody (spartalizumab) and experienced a durable objective response with regression of both injected and non-injected lesions.

Methods We analyzed pretreatment and post-treatment tumor and peripheral blood samples from our patient with single-cell RNA sequencing, 30-parameter flow cytometry, T cell receptor sequencing, and multiplexed immunohistochemistry. We analyzed cancer-specific CD8 T cells using human leukocyte antigen (HLA)-I tetramers loaded with MCPyV peptides. We also analyzed STING expression and signaling in the tumor microenvironment (TME) of 88 additional MCC tumor specimens and in MCC cell lines.

Results We observed high levels of MCPyV-specific T cells (12% of T cells) in our patient's tumor at baseline. These cancer-specific CD8 T cells exhibited characteristics of exhaustion including high TOX and low TCF1 proteins. Following treatment with STING-agonist plus anti-PD-1, IT CD8 T cells expanded threefold. We also observed evidence of likely improved antigen presentation in the MCC TME (greater than fourfold increase of HLA-I-positive cancer cells). STING expression was not detected in any cancer cells within our patient's tumor or in 88 other MCC tumors, however high STING expression was observed in immune and stromal cells within all 89 MCC tumors.

WHAT IS ALREADY KNOWN ON THIS TOPIC

⇒ Stimulator of interferon genes (STING) agonists have shown promise in preclinical cancer models by activating CD8 T cells^{13 14} and initiating both local and systemic anticancer responses. However human mechanistic studies remain limited.

WHAT THIS STUDY ADDS

⇒ This study of a patient with excellent response to intratumoral STING agonism demonstrates increased expression of antigen presentation genes and non-specific T cell expansion likely driven by innate immune cells present in the tumor microenvironment prior to therapy.

HOW THIS STUDY MIGHT AFFECT RESEARCH, PRACTICE OR POLICY

⇒ This study suggests that STING agonist therapies may be particularly effective in tumors that evade immune detection by downregulating antigen presentation. Future clinical trials and biomarker studies could benefit from focusing on this mechanism to refine therapeutic strategies.

Conclusions Our results suggest that STING agonists may be able to work indirectly in MCC via signaling through immune and stromal cells in the TME, and may not necessarily need STING expression in the cancer cells. This approach may be particularly effective in tumors that are already infiltrated by inflammatory cells in the TME but are evading immune detection via HLA-I downregulation.

INTRODUCTION

Innate immune sensors of pathogen-associated molecular patterns (PAMPs) represent an important host defense mechanism against infectious agents and have been employed as targets in several oncology clinical trials to stimulate anticancer immunity.¹



Stimulator of interferon genes (STING) protein is a PAMP sensor that appears to be a promising target in preclinical mouse models.^{2–5} The STING pathway senses cytoplasmic DNA through cyclic guanosine monophosphate–adenosine monophosphate (GMP-AMP) synthase (cGAS), which then produces cyclic GMP-AMP as a secondary messenger. This in turn acts on STING protein to induce transcription of type I interferons and inflammatory cytokines via nuclear factor κB and interferon regulatory factor 3.³ The STING pathway is thought to have evolved to protect against double-stranded DNA viruses that replicate in the cytoplasm of cells; however, it can also be engaged by DNA-damaging chemotherapies and radiation that cause DNA release into the cytoplasm.^{6,7} Murine models have shown that these DNA-damaging therapies lead to adaptive anticancer immune responses, primarily through activation of STING in dendritic cells in the tumor microenvironment (TME).^{6,8} Based on these findings, several novel agents designed to directly engage STING have been developed.^{9–12} These STING agonists, when delivered intratumorally (IT), appear to increase IT infiltration of natural killer (NK) cells, activate CD8 T cells^{13,14} and facilitate both local and systemic anticancer responses.

While IT administration of STING agonists has been successful in murine models, recent clinical trials have yielded disappointing results. In a clinical trial (NCT02675439) of IT ADU-S100 monotherapy in 47 patients with metastatic tumors, only 1 patient had a confirmed response.¹¹ Of note, the only responding patient had a diagnosis of Merkel cell carcinoma (MCC). In a separate trial (NCT03172936) of IT ADU-S100 in combination with intravenous anti-programmed death (PD)-1 (spartalizumab) in 106 patients with metastatic tumors, only 11 patients responded (objective response rate of 10%) with 10 patients achieving a partial response (PR) and 1 patient receiving a complete response (CR).¹⁰ One of those 11 responders also had a diagnosis of MCC and is the subject of this report.

MCC is a rare neuroendocrine cancer associated with Merkel cell polyomavirus (MCPyV; a double-stranded DNA virus) and/or ultraviolet radiation exposure, and usually occurs in older and/or immunosuppressed patients.¹⁵ Both MCPyV-positive (VP) and MCPyV-negative (VN) MCC tumors are considered immunogenic with excellent prognosis in patients with brisk IT infiltration of CD8 T cells.¹⁶ Both MCC subsets have a particularly high response rate to agents that block PD-1 or its ligand (PD-L1), with around half of patients experiencing durable responses.^{17–20} However, for patients with PD-(L)1 refractory MCC tumors, there is a strong unmet need for effective therapies. Unlike most other cancers, VP-MCC allows unique opportunities to study cancer-specific immune responses because MCPyV-specific CD8 T cells can be isolated across patients using peptide-major histocompatibility complex (MHC) multimers. This approach can provide insight into mechanisms of response and failure for immunotherapies.

Here, we describe the clinical course along with detailed biomarker analyses of a patient with metastatic VP-MCC, refractory to avelumab (anti-PD-L1 antibody) treatment, who experienced durable clinical response in both injected and non-injected lesions with combination treatment of IT STING-agonist (ADU-S100) plus intravenous anti-PD-1 (spartalizumab). To further assess the relevance of our findings to patients with MCC in general, we also determined STING expression and activity in other MCC tumor samples and cell lines.

RESULTS

Clinical MCC history and response to STING agonist and anti-PD-1

A patient in their 60's presented with a primary VP-MCC tumor located on the left knee along with draining inguinal lymph node metastasis, which was initially treated with surgery and adjuvant radiotherapy (figure 1A). One month later, they developed distant metastatic disease in the left elbow region. They received systemic treatment with intravenous avelumab, which resulted in a CR. Avelumab was electively discontinued after completing 1 year of therapy. Nine months later, the patient developed recurrence with multifocal MCC metastases in the left lower extremity, which were refractory to a 6-month long retreatment with avelumab.

The patient was subsequently enrolled in the above-mentioned clinical trial (NCT03172936) and received IT injections of the STING agonist (ADU-S100) with intravenous spartalizumab, both administered every 4 weeks. They experienced quick-onset clinical benefit with rapid regression of both injected and non-injected lesions, starting soon after the first treatment, leading to an overall PR (43% reduction in size of target lesions; figure 1B), per Response evaluation criteria in solid tumors (RECIST) V.1.1. After only two administrations of ADU-S100, there were no residual injectable lesions and hence IT ADU-S100 was discontinued. After experiencing disease control for 1 year, the patient experienced MCC progression again with new metastases in the left lower extremity (figure 1B) and started another systemic therapy.

During the course of their treatment, we collected serial tumor biopsies and peripheral blood specimens to characterize antitumor immune response via detailed immunophenotyping of MCC cancer and immune cells, including cancer-specific CD8 T cells, both in the TME and peripheral blood samples.

IT STING agonism increased T cell infiltration into MCC tumors

We first performed single-cell RNAseq (scRNAseq) with feature barcoding (CITEseq) on pretreatment and post-treatment tumor and blood specimens in an unbiased approach to study cell populations and gene expression profiles at various time points. DNA barcoded human leukocyte antigen (HLA)-I tetramers containing MCPyV or bystander cytomegalovirus (CMV) and Epstein-Barr

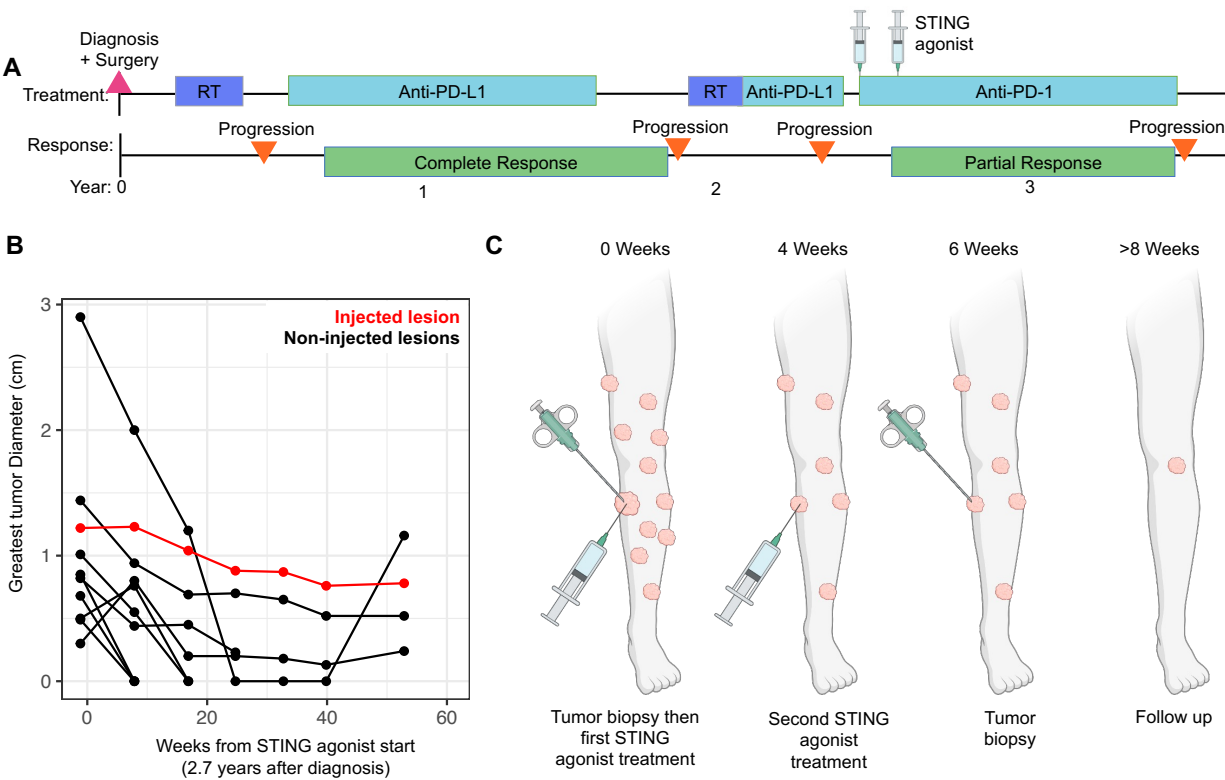


Figure 1 Clinical MCC course and characterization of partial response to intratumoral STING agonist+intravenous anti-PD-1 therapy. (A) Schematic of clinical course of a patient in their 60's with multifocal metastases on left lower extremity (LLE) from MCPyV+MCC, which had progressed on prior PD-(L)1 blockade. They were enrolled on a clinical trial (NCT03172936) and received two intratumoral injections of the STING agonist (ADU-S100) plus intravenous anti-PD-1 (spartalizumab), both administered every 4 weeks. The patient experienced rapid-onset regression of both injected and non-injected lesions, with durable partial response maintained for 53 weeks before developing progression. (B) Size of injected and non-injected tumors on the LLE throughout the time course depicts a partial response to therapy with an overall decrease in disease burden of 43%. The injected tumor is shown in red with non-injected tumors in black. (C) Representative CT and PET/CT images of LLE lesions are shown prior to, during, and at the time of disease progression. MCC, Merkel cell carcinoma; MCPyV, Merkel cell polyomavirus; PD-1, programmed cell death protein-1; PD-(L)1, programmed death-ligand 1; PET, positron emission tomography; RT, radiotherapy; STING, stimulator of interferon genes.

virus (EBV) peptides were used to identify antigen-specific T cells (figure 2).²¹ We then designed a 27-fluorophore flow cytometry panel to further refine the initial observations from the CITEseq studies and to also allow the identification of rare cell populations that could have been missed due to the lower number of cells that can be analyzed via scRNAseq (figure 2A).

Unbiased clustering and dimensionality reduction in the pretreatment (baseline) tumor biopsy revealed the TME composition of 70% cancer cells and 28% immune cells, with the remaining 2% of cells bearing markers of stromal/endothelial cells including CD34. 95% of immune cells were in the T cell, NK cell or dendritic cell clusters, with other cells such as B cells, tumor-associated macrophages and neutrophils being relatively rare. Meanwhile, cancer cells are primarily grouped into two distinct clusters of proliferating and non-proliferating cells, as differentiated by Ki67 expression.

Following IT STING agonist injection, cancer cells decreased from 70% to 49% of the TME, while all T cells (CD4 and CD8) increased twofold from 18%

to 36% (figure 2B and C). Further subclustering of MCC cancer cells, T cell and myeloid populations (figure 2, online supplemental figures 1–3) revealed that while both cancer cell populations decreased over the course of immunotherapy, the most dramatic change was in the proliferating cancer cells, which decreased from 17% of all cells in the TME before treatment to 5% following treatment (figure 2D). Subclustering of T cells revealed that memory CD4 T cells, Regulatory T cells (T_{REG}), CLA+CD8 T cells, progenitor exhausted, and terminally exhausted CD8 T cells each comprised more than 2% of the cells in the TME prior to STING treatment. All T cell populations increased proportionally following treatment without major phenotypic changes (figure 2E). No significant changes were observed in myeloid cells. However, a high portion of myeloid cells were plasmacytoid dendritic cells (2.7% of pretreatment cells, marked by CD123 expression), which are thought to specialize in sensing some PAMPs. An additional 2% of cells in the TME were classical dendritic cells

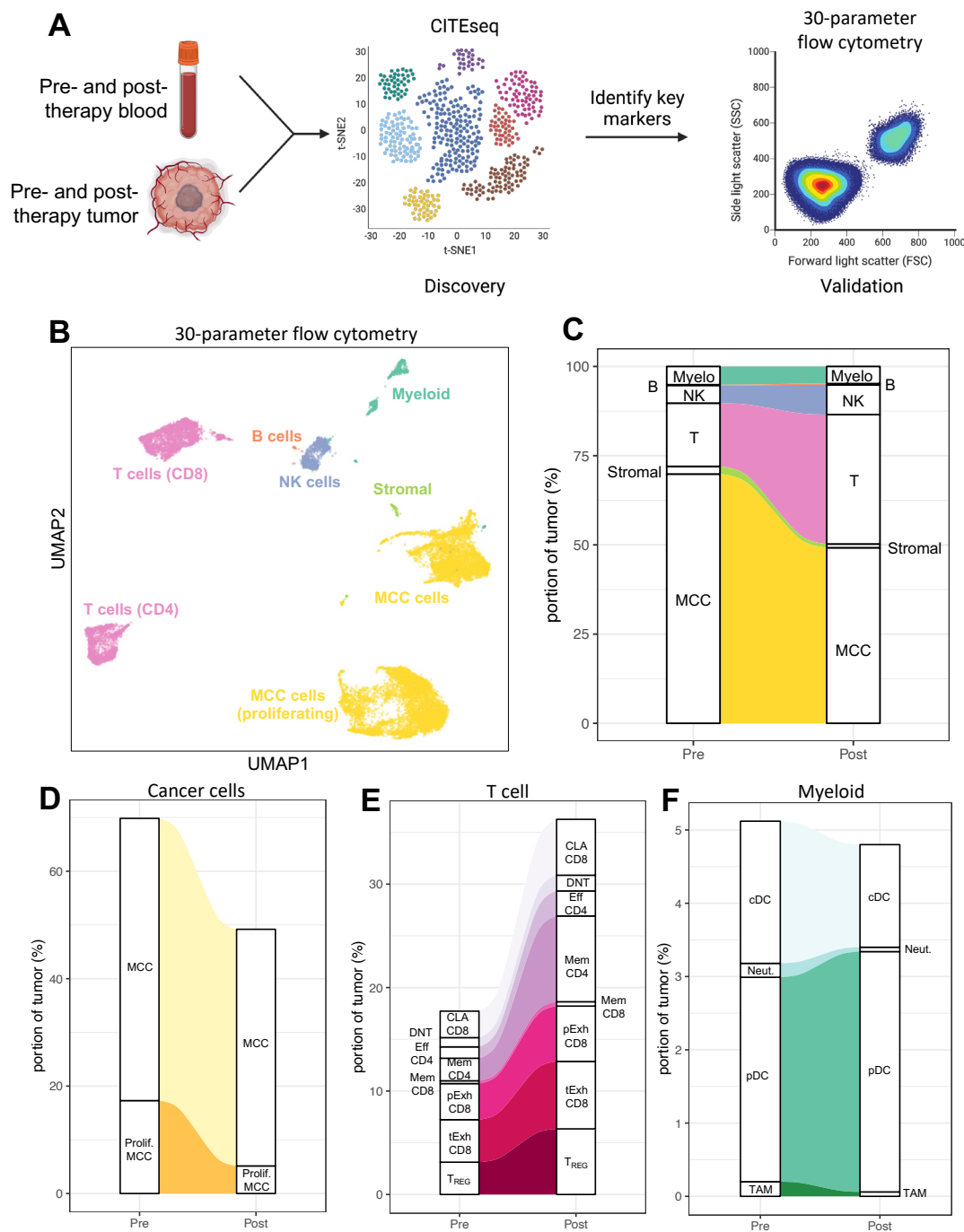


Figure 2 Intratumoral T cells increase following intralesional STING agonism. (A) Experimental overview. CITEseq was performed on pretreatment and post-treatment tumor and blood specimens for unbiased analyses. Key markers and cell populations were identified and used to design a 30-parameter flow cytometry panel to validate samples in high throughput fashion to capture rare cell populations. (B) UMAP plot of 30-parameter flow cytometry data from pre-STING and post-STING agonist treatment. Each point represents one cell colored by cell lineage. Samples were subsetted to 10,000 cells per time point for visualization purposes. (C) Alluvium plot of tumor composition before and after STING agonism showing expansion of T cells and contraction of cancer cells following treatment with STING agonist. (D) Alluvium plot of cancer cells subclustered into proliferating MCC and non-proliferating cells showing contraction of both populations. (E) Alluvium plot of T cells showing an expansion of T cells following STING agonism. All T cells expanded similarly regardless of phenotype. (F) Alluvium plot of myeloid cells before and after STING agonist treatment. A predominance of plasmacytoid dendritic cells was noted but minimal changes occurred over the course of therapy. cDC, classical dendritic cells; CITEseq, feature barcoding; CLA, cutaneous lymphocyte antigen; DNT, double negative T cells; Eff, effector; MCC, Merkel cell carcinoma; Mem, memory; Myelo, myeloid cells; Neut, neutrophils; NK, natural killer cells; pDC, plasmacytoid dendritic cells; pExh, progenitor exhausted; prolif, proliferating; STING, stimulator of interferon genes; TAM, tumor associated macrophages; tExh, terminally exhausted; T_{REG}, Regulatory T cell; t-SNE, t-distributed stochastic neighbor embedding; UMAP, Uniform Manifold Approximation and Projection.

(marked by high CD11c expression). Both dendritic cell populations expressed high levels of STING protein (online supplemental figure 3).

Cancer-specific CD8 T cells expand in tumors following IT STING agonism

Given the overall increase in T cells observed following STING agonism, we sought to characterize the dynamics of antigen-specific T clones in the tumor and blood using a dual approach schematized in figure 3A. T cell specificity was identified using DNA barcoded HLA-I tetramers (with MCPyV, CMV or EBV peptides) with paired CITEseq and T-cell receptor (TCR) variable-diversity-joining (V(D)J) sequencing (figure 3B). Cancer-specificity of multimer-positive cells was further supported by visualizing CD39 positivity in these cells, known to be elevated in IT cancer-specific T cells.²² This resulted in 12 T cell clonotypes specific for MCPyV in a B*37:01 allele. CD8 T cells specific for other MCPyV or other viral epitopes were detected at low levels, and antigen-specific TCRs could not confidently be identified.

T cell clonal frequency was quantified using bulk beta TCRseq (figure 3C). This approach revealed that bulk T cells (CD4 and CD8) expanded from 3.3% of the TME before STING agonism to 13% after agonism, similar to the T cell expansion measured using flow cytometry. This expansion appeared to be non-specific as all T cell clones expanded roughly proportionately, regardless of T cell specificity. Greater than 99% of 5,128 clonotypes did not significantly change in proportion following treatment. Specifically, only 8 of 5,128 IT clones increased in a statistically significant manner following treatment and 20 of 5,128 clones significantly decreased as a portion of all T cells (expanded/contracted clones determined by beta-binomial test with p value < 0.01; see Methods and online supplemental figure 4).

While the aforementioned approach quantified T cells of unknown specificity, we also sought to quantify cancer-specific T cells in pretreatment and post-treatment tumors. This was done by annotating the bulk TCRseq data with TCR sequences of known specificity derived from CITEseq and MHC multimers. This analysis revealed that cancer-specific CD8 T cells expanded from 0.39% of all cells in the TME prior to STING agonism to 0.93% of all cells in the TME after agonism. However, this was again largely driven by non-specific T cell expansion as 11.7% of T cells in the TME before STING agonist treatment and 7.2% of T cells after treatment were specific for the B*37:01 MCPyV epitope (figure 3C). Individual cancer-specific T cell clones did undergo some dynamic changes with 1 of 12 cancer-specific clones expanding following STING treatment and 2 of 12 contracting as a portion of all T cells (online supplemental figure 4). Cancer-specific T cells were long-lived in the blood and were detected 1 year after treatment (at the time of recurrence) at frequencies similar to pretreatment (0.04% of all peripheral blood mononuclear cells (PBMC)).

Cancer-specific CD8 T cells exhibit characteristics of exhaustion

We next sought to phenotype cancer-specific T cells in the tumor and blood. Unbiased clustering of scRNAseq of CD8 T cells yielded clusters of memory, naïve, progenitor exhausted, terminal exhausted, two effectors, and two gamma delta populations (figure 4A and B). Expression of stem-like and memory genes was higher in CD8 T cells in blood, while genes associated with exhaustion were higher in tumor tissues and highest in cancer-specific T cells (figure 4C). Cancer-specific CD8 T cells in tumors were largely confined to the terminally exhausted population defined by high expression of *PDCD1* (PD-1) and *ENTPD1* (CD39) (figure 4B and D). The proportion of IT cancer-specific CD8 T cells in the terminally exhausted population decreased slightly following STING agonism, but low numbers of cancer-specific CD8 T cells in the pretreatment time point limited these analyses (figure 4D). To circumvent the low capture efficiency of scRNAseq, flow cytometry was subsequently used as a higher throughput technique. These data show high expression of TOX, TCF7 and PD-1 proteins in IT cancer-specific CD8 T cells (99% PD-1+, 99% TOX+, 14% TCF1+, in pretreatment samples, figure 4E). This was unchanged following STING agonism suggesting that treatment did not induce lasting phenotypic changes in IT cancer-specific CD8 T cells.

MCC cancer cells are STING deficient

To study the effects of IT ADU-S100 on cancer, immune and stromal cells in the TME, we first analyzed STING expression in the TME by performing multiplexed immunohistochemistry (mIHC) on the studied patient's tumor specimen. Previous studies of STING in MCC have suggested that this pathway is deficient in VP-MCC.²³ We confirmed that the STING protein was indeed absent in the MCC cancer cells, with mIHC staining showing STING expression in immune and stromal cells, but an absence of STING protein in cancer cells (figure 5A). This pattern of STING expression was then confirmed broadly in further staining of 88 MCC tumors from 68 unique patients (55 VP, 13 VN), which similarly showed an absence of STING expression in cancer cells (figure 5B).

The absence of STING protein in cancer cells suggests that the downstream effects of STING-agonism using ADU-S100 are likely mediated by effects on the non-cancer cells rather than the MCC cancer cells in the TME. To independently confirm that MCC cells do not respond to ADU-S100 treatment, four VP-MCC cell lines were treated with increasing doses of ADU-S100 (figure 5C). Treatment did not induce the production of interferon beta (a downstream target of STING activation) in MCC cell lines, but led to the production of interferon beta in control monocytic THP-1 cells (figure 5C). Moreover, none of the MCPyV-driven MCC cell lines that were tested produced detectable amounts of STING protein (figure 5C).

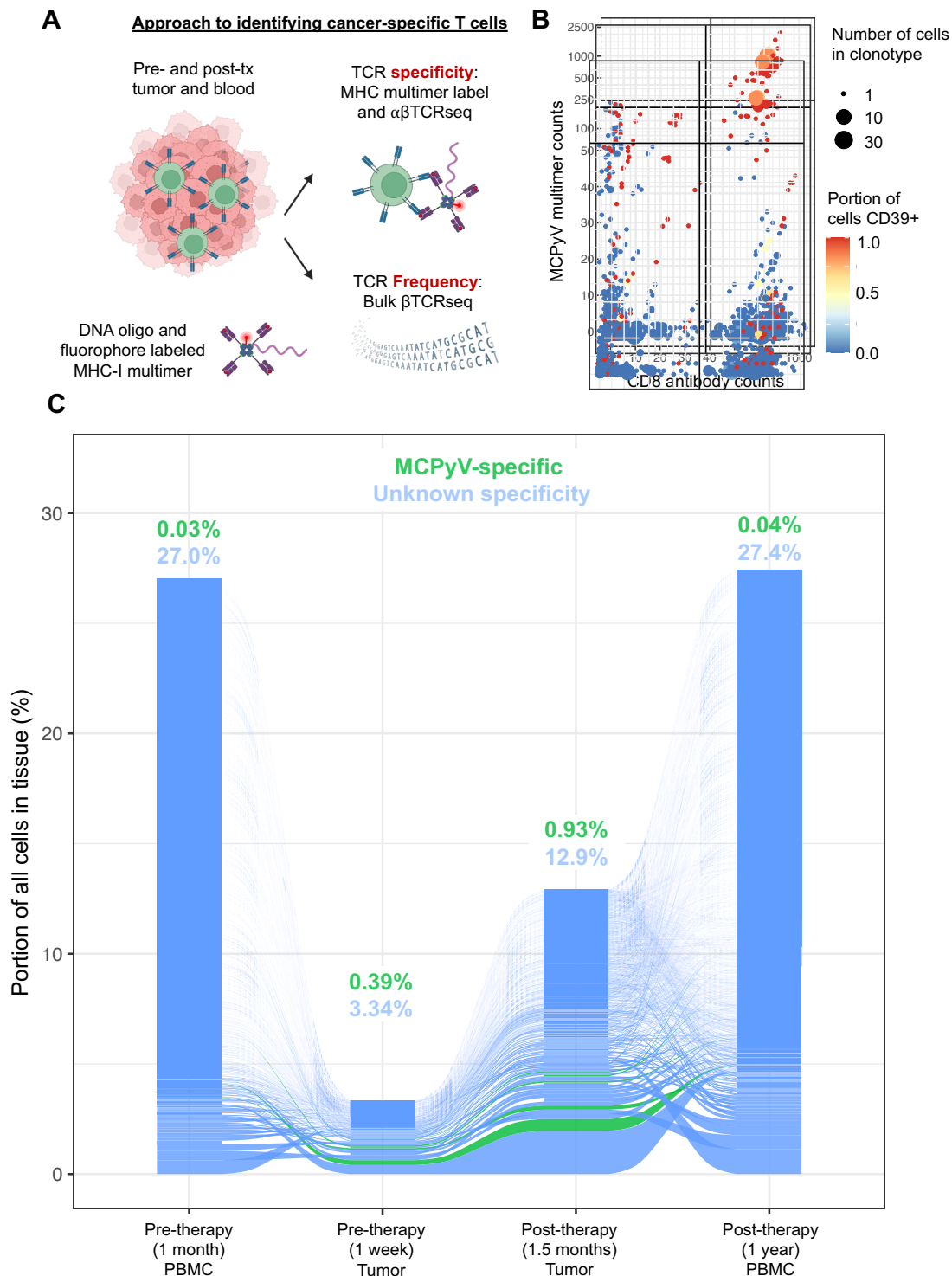


Figure 3 Intralesional STING treatment increases cancer-specific intratumoral T cell frequency. (A) Schematic of approach to quantifying frequency of MCPyV-specific CD8 T cells in tumor and blood specimens. Tumor or blood specimen were stained with DNA oligo and fluorophore labeled MHC tetramers and CITEseq with V(D)J seq was performed to identify specificity of TCRs. In parallel, beta-TCRseq was performed on tumor and blood specimens to quantify frequency of TCR clonotypes. (B) Gating of MCPyV-specific CD8 T cells via CITEseq. All cells with a single productive alpha and single productive beta TCR are shown. Cells with identical TCR sequences were grouped as clonotypes. X axis represents the median counts of CD8 antibody for each clonotype and y axis represents the median counts of an HLA-B*37:01 multimer containing a T antigen peptide. (C) Frequency of T cell clonotypes in tumor and blood before and after intralesional STING agonism. Alluvium plot where each alluvium represents an individual T cell clonotype. Clonotypes known to be MCPyV-specific are green. MCPyV-specific CD8 T cells were present in tumor and blood of patient. CITEseq, feature barcoding; HLA, human leukocyte antigen; MCPyV, Merkel cell polyomavirus; MHC, major histocompatibility complex; PBMC, peripheral blood mononuclear cells; STING, stimulator of interferon genes; TCR, T-cell receptor; tx, treatment; V(D)J, variable–diversity–joining.

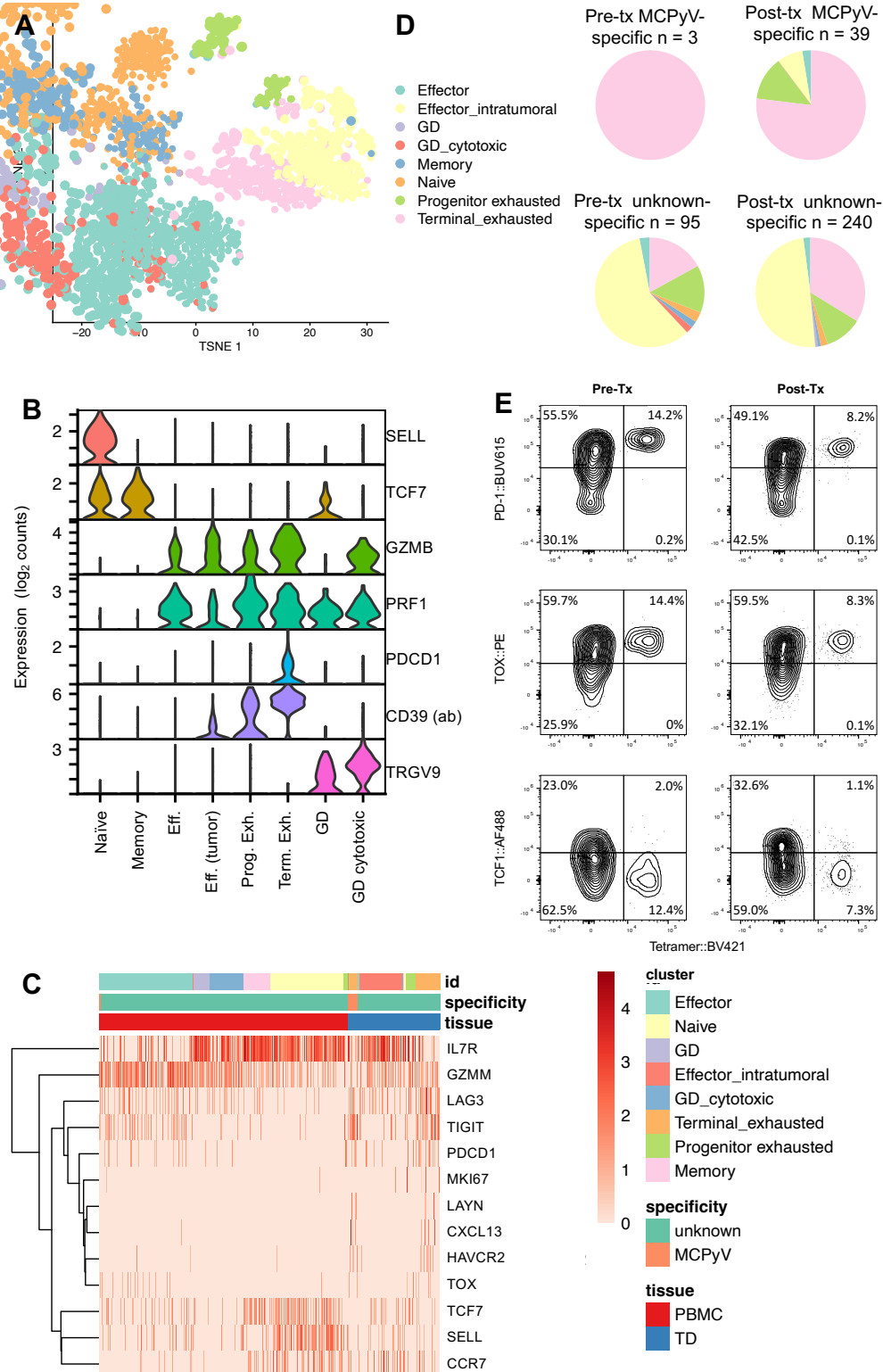


Figure 4 Cancer-specific CD8 T cells exhibit characteristics of exhaustion. (A) TSNE plot of CD8 T cells isolated in silico from single-cell RNAseq of patient tumor and blood specimens. Cells are colored by cluster. (B) Violin plots of expression of key genes in each cluster. Each row represents gene expression except for CD39 which is protein expression. (C) Heatmap of single-cell RNAseq data of CD8 T cells from tumor or blood specimen. (D) Portion of MCPyV-specific CD8 T cells in tumors in each of eight clusters. MCPyV-specific CD8 T cells in top pie charts and CD8 T cells of unknown specificity in bottom charts. Pretreatment specimen on left hand side and post-treatment on right. N in each pie chart represents number of CD8 T cells that are cancer-specific (top) or of unknown-specificity (bottom). (E) FACS plots of CD8 T cells from tumors showing expression of proteins associated with exhaustion or stem like phenotypes in cancer-specific T cells. Eff., effector; FACS, fluorescent activated cells sorting; GD, gamma delta T cells; MCPyV, Merkel cell polyomavirus; PBMC, peripheral blood mononuclear cells; PD-1, programmed cell death protein-1; TD, tumor digest; t-SNE, t-distributed stochastic neighbor embedding; tx, treatment.

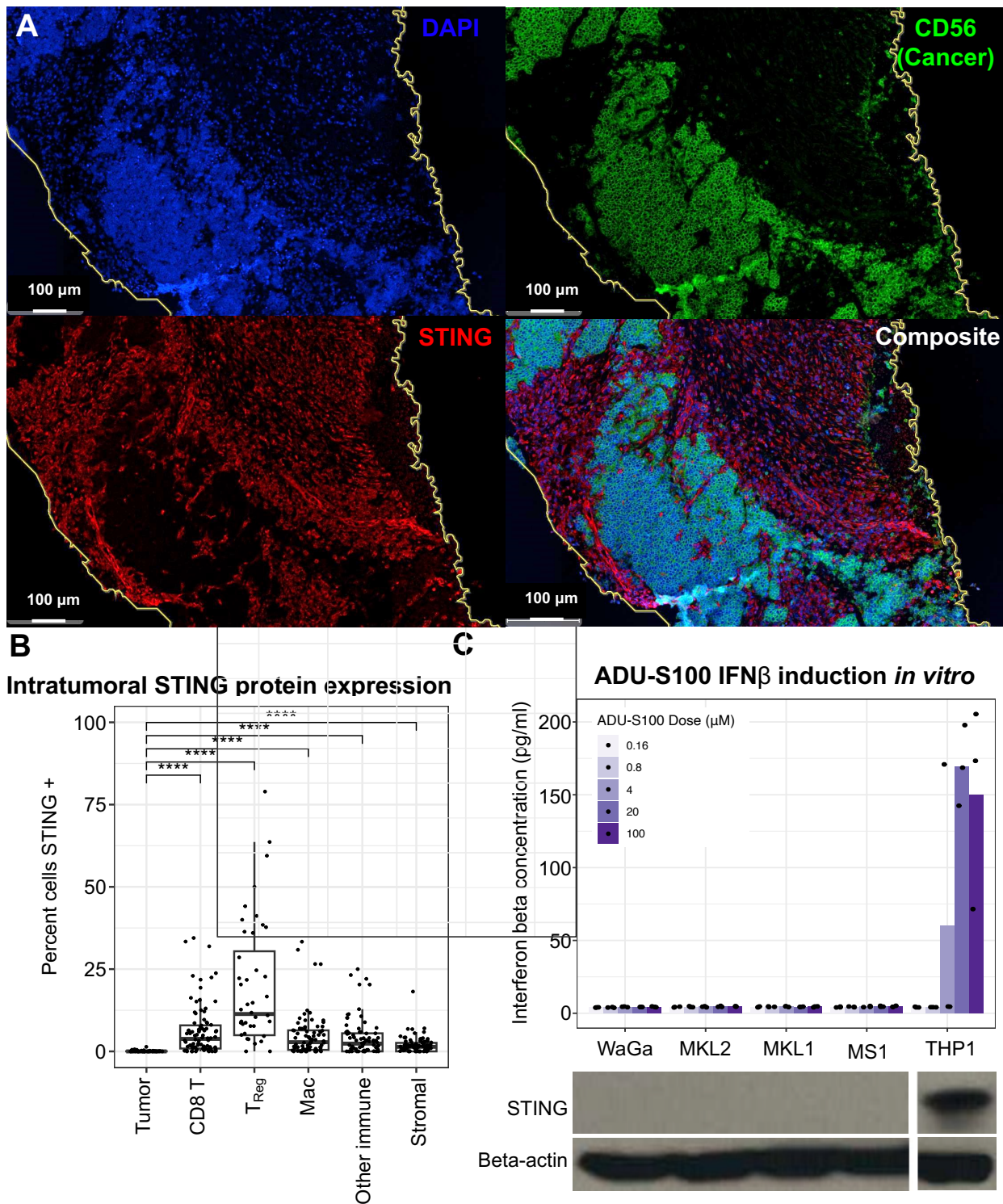


Figure 5 Merkel cell carcinoma cancer cells are deficient in STING signaling. (A) Multiplexed immunohistochemistry of post-ADU-S100 treated tumor. Areas of CD56 positivity (representing MCC cancer cells) are non-overlapping with STING positivity, which is primarily expressed in stromal and immune tissues. (B) Quantification of STING expression. Each point represents 1 of 88 unique tumor specimens on a tissue microarray. STING is universally absent in MCC cancer cells. Cancer cells defined as CD56+, CD45-, CD8 T cells defined as CD8+, T_{Reg} cells defined as CD4+, FoxP3+, macrophages defined as CD68+ or CD163+, other immune cells defined as CD45+ cells which did not fall into prior categories, stromal cells defined as CD45-, CD56- cells. Statistical comparison with one-way ANOVA compared with tumor expression. *p<0.05, **p<0.01, ****p<0.0001, NS (not significant). (C) MCC cell lines do not produce interferon-beta in response to ADU-S100 treatment. WaGa, MKL-2, MKL-1, MS1 MCC cells and THP1 cells (control human monocytic cells) were all treated with decreasing doses of ADU-S100. None of the MCC cell lines produced detectable interferon-beta at any tested ADU-S100 concentration. These cells were all also deficient in STING protein (western blot, below). ANOVA, analysis of variance; 4',6-diamidino-2-phenylindole (DAPI); Mac, macrophage; MCC, Merkel cell carcinoma; STING, stimulator of interferon genes; T-Reg, Regulatory T cell.

Cancer cells upregulate HLA following IT STING agonism

To investigate the mechanisms of anticancer immune responses following STING agonism, we investigated the expression of genes associated with antigen processing and presentation (figure 6A). MCC cancer and non-cancer cells were isolated *in silico* (online supplemental figure 5) and a gene set of 18 genes associated with antigen presentation was used to measure this pathway in aggregate. A 49% increase in this gene signature was observed in cancer cells following STING agonism ($p < 10^{-16}$). A more modest 4% increase was observed in non-cancer cells in the TME ($p = 0.016$) with higher expression of antigen presentation genes in non-cancer cells than in cancer cells.

Further analyses of these genes showed that most of this increase was driven by beta-2 microglobulin (online supplemental figure 5), which was significantly upregulated in cancer cells following STING treatment ($p < 10^{-16}$; figure 6B). However, no remarkable change was observed in other cells in the TME. Upregulation of HLA-I was validated at a protein level via fluorescent activated cells sorting (FACS), which showed 1.8% of cancer cells positive for HLA-I prior to STING treatment compared with 8.2% following STING treatment. Consistent with these findings, we observed increases in genes associated with interferon gamma or interferon alpha receptor signaling in most cell types in the TME following STING agonism (online supplemental figures 6A&B) suggesting that these cytokines were more active in the TME after STING agonism.

DISCUSSION

STING agonists have shown great promise in preclinical models.^{3,24,25} However, clinical trials have shown limited early efficacy with objective response rates reported between 2% and 10%.^{10,11} It is of note that 2 of 4 (50%) patients with MCC treated on two large trials of ADU-S100 (NCT02675439; NCT03179236) experienced objective responses compared with 12 of 149 (8%) patients with non-MCC. Intrigued by the seemingly higher response rate in MCC, we performed exhaustive biomarker studies on a patient with metastatic MCC tumors that were refractory to anti-PD-L1 therapy. This patient with numerous (>10) metastatic tumors received only two IT injections of STING-agonist (ADU-S100) in their lower extremity plus systemic anti-PD-1 therapy and experienced a durable objective response in both injected and non-injected (distant) lesions. Regression of cancer cells in the TME was accompanied by a concomitant increase in the proportion of inflammatory cells, likely through cytokine production by non-cancer (immune) cells in response to STING-agonism.

Durable objective response, including abscopal tumor regression in non-injected lesions, in our patient suggested that STING-agonism in the injected tumor facilitated a systemic adaptive immune response. To further interrogate this, we used a panel of MCPyV-specific

HLA-I multimers to leverage the viral etiology of this patient's tumor to study cancer-specific T cells. Indeed, we observed a 2.4-fold increase in cancer-specific T cells in the TME following STING agonism. Using scRNAseq and FACS to further determine the characteristics of this expansion, we found that 93% of cancer-specific CD8 T cell clonotypes in the tumor following STING agonism had at least one cell detected in the pretreatment tumor. This suggests that priming of naïve T cells or recruitment of peripheral T cells may not have been a major driving factor in our patient's anticancer immune response. Furthermore, minimal changes were detected in cancer-specific T cell phenotype or exhaustion status suggesting that a reversal of CD8 T cell exhaustion was also not a major mechanism here. We did however note an increase in HLA-I positive cancer cells from 1.8% before treatment to 8.2% after treatment consistent with ADU-S100 upregulating antigen presentation in cancer cells. Since disruption of the antigen-presentation pathway is a well-known immune evasion mechanism in MCC, this may have been relevant to the successful clinical response in our patient.^{26–29} STING agonism may be a potentially promising approach to overcome this particular mechanism of immune evasion and improve the visibility of cancer cells to the immune cells in PD-(L)1 refractory MCC tumors.

We then asked if STING agonism may be acting directly on the STING pathway in the MCC cancer cells. Since a recent *in vitro* study had suggested that MCC tumors are likely STING deficient,²³ we examined STING expression by mIHC in our patient treated with ADU-S100 and found STING expression to be absent in the MCC cancer cells, but intact in the non-cancer (immune) cells. We then verified the lack of STING expression in MCC cancer cells in a large independent patient cohort (88 MCC tumors in 68 patients, including both VP and VN MCC). It has been proposed that inactivation of STING is an important part of immune evasion by MCPyV, a DNA virus. Indeed, the Leu-X-Cys-X-Glu (LxCxE) motif that inactivates STING in adenovirus and human papillomavirus³⁰ is also present in the MCPyV large T antigen.³¹

Murine studies of STING's role in anticancer immunity have shown that STING activity is vital in dendritic cells, but largely dispensable in cancer cells.^{6,8} These dendritic cells would release interferons following STING signaling, which in turn upregulates HLA-I on cancer cells, recruits immune cells into the tumors, stimulates adaptive immunity and mediates tumor regression. We observed a high portion of plasmacytoid dendritic cells (pDC) in the treated patient's tumor (2.7% of all cells in the TME prior to treatment). This is compared with only 0.1% (median) of cells expressing pDC markers in a prior study of 22 MCC tumors.³² It is plausible that a relative abundance of pDC in the TME may predict success with IT STING agonism, and future biomarker studies in trials of STING agonists should investigate this further.

Although initial trials of STING agonists have yielded relatively low response rates; here, we show that these agents with anti-PD-1 therapy can lead to durable immune

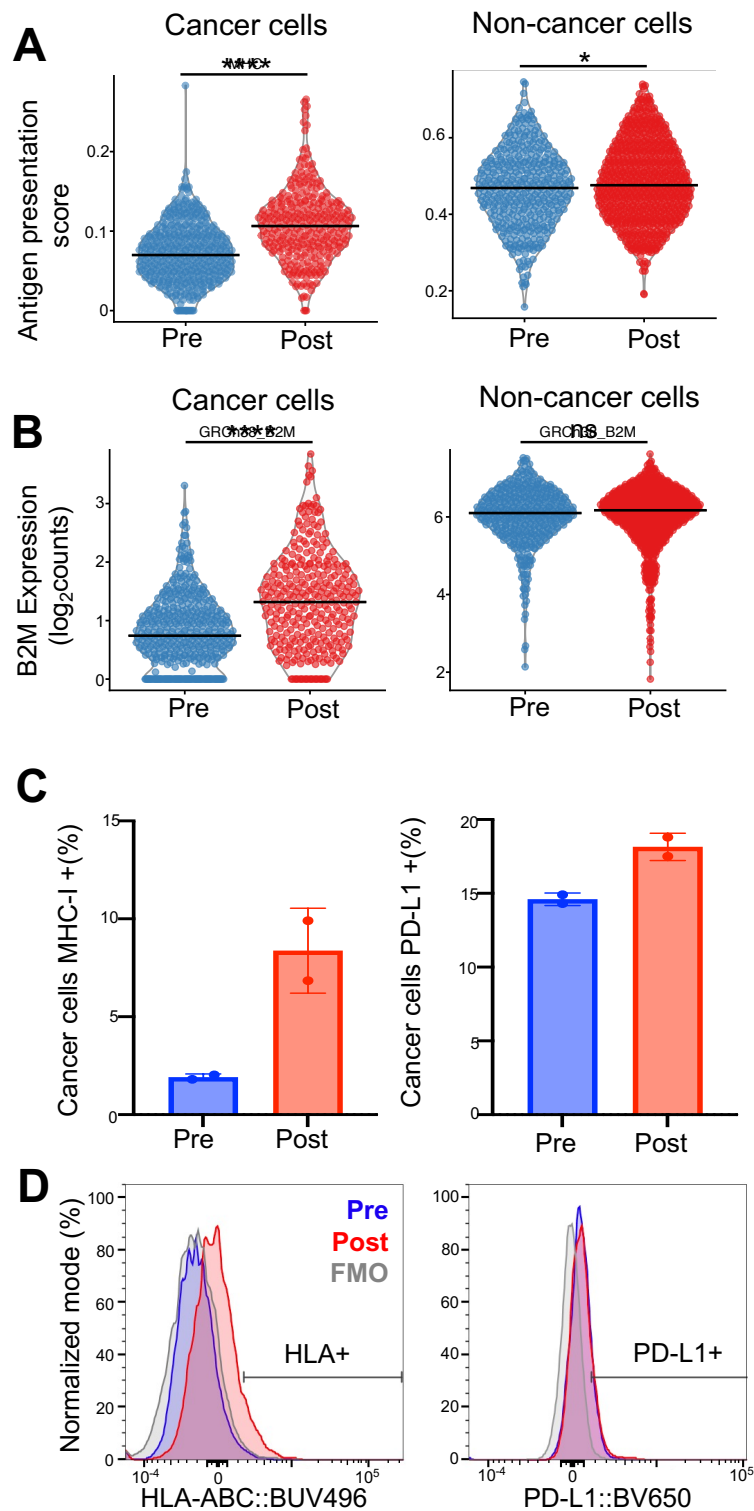


Figure 6 MCC cancer cells upregulate HLA following STING agonism. (A) scRNAseq data showing upregulation of antigen presentation genes following STING agonism on cancer cells, cancer or non-cancer cells identified in silico. Antigen presentation score calculated using 16 genes involved in the HLA-I antigen presentation pathway. (B) B2M upregulation in cancer cells but not non-cancer cells following STING agonism. (C) Quantification of HLA-I and PD-L1 expression on cancer cells via flow cytometry. Each data point represents one of two technical replicates. (D) FACS plot of HLA expression (left) or PD-L1 expression (right) on cancer cells before and after IT STING agonist treatment. T-tests with Bonferroni multiple comparison testing used for statistical significance. P value key: ns= $p > 0.05$, * $p < 0.05$, ** $p < 0.01$, *** $p < 0.001$, **** $p < 0.0001$. B2M, beta-2 microglobulin; FACS, fluorescent activated cells sorting; FMO, fluorescence minus one; HLA, major histocompatibility complex; IT, intratumoral; MCC, Merkel cell carcinoma; MHC, major histocompatibility complex; ns, not significant; PD-L1, programmed death-ligand 1; scRNAseq, single-cell RNAseq; STING, stimulator of interferon genes.

responses in the PD-(L)1 refractory setting. We show that a successful anticancer immune response via STING agonism does not need STING expression in the targeted cancer cells. Our results raise the possibility that STING agonism could be effective in tumors that already are infiltrated by inflammatory cells in the TME, but are evading immune detection via HLA-I downregulation. Further in vivo studies are required to discern the mechanism(s) underlying successful responses to STING agonism.

METHODS

Study design and participants

Samples were collected with informed consent for research use and were approved by the Fred Hutch Cancer Center institutional review board, in accordance with the Declaration of Helsinki (2013) as part of observational registry studies focusing on MCC (Fred Hutch Cancer Center IRB#6585). This patient presented to our institution as part of the standard of care. On progression on anti-PD-L1, they were evaluated and enrolled in a clinical trial with ADU-S100 and spartalizumab antibody¹⁰ (NCT03179236). ADU-S100 was administered at 3200 mcg/injection every 4 weeks. One lesion was injected in the first cycle, and a separate lesion was injected in the second cycle. Tumor biopsy was taken 6 weeks after the first lesion was injected. Blood was collected before and 1 year after treatment. Every 4 weeks, the patient received spartalizumab administered at a dose of 400 mg until progression.

Blood collection and processing

Heparinized whole blood from patients with MCC was processed at the Specimen Processing Lab (Fred Hutchinson Cancer Center). PBMC were isolated by routine Ficoll density gradient centrifugation and cryopreserved in liquid nitrogen.

Tumor digestion processing

Fresh MCC tumor specimens from needle cores, punch biopsies, or surgical excisions were enzymatically digested as described.³³ All single-cell suspensions were cryopreserved in freezing medium (50% human serum (Valley Biomedical), 40% RPMI (Corning), and 10% DMSO (Sigma-Aldrich)) in liquid nitrogen.

Flow cytometry

Frozen pretreatment and post-treatment PBMC and tumor digest samples were analyzed using flow cytometry as described elsewhere.³⁴ Briefly, tubes were thawed at 37°C and mixed with complete media. DNase I (10 units/ml) was added and samples were left to rest for an hour. Cells were counted and divided into 1–3 million cells per tube. After two washes with phosphate-buffered saline (PBS), dasatinib (100 nM) and live dead dye (Live dead Blue; Thermo Fisher) were added and the samples were incubated at 37°C for 10 min. HLA-I multimers were added, followed by cell surface receptor

antibodies (BV605 conjugated anti-E selectin (68-5 H11; BD), BUV395 conjugated anti-CD56 (NCAM16.2; BD), BUV615 conjugated anti-PD1 (EH12.1; BD), BV650 conjugated anti-PDL1 (29E.2A3; BioLegend), PE-Cy7 conjugated anti-CLA (HECA-452; BioLegend), BV785 conjugated anti-CD163 (GHI/61; BioLegend), BUV805 conjugated anti-CD4 (SK3; BD), BV570 conjugated anti-CD8 (RPA-T8; BioLegend), BV711 conjugated anti-HLA-DR (L243; BioLegend), APC-Fire750 conjugated anti-CD123 (S18016F; BioLegend), BUV563 conjugated anti-CD14 (MφP9; BD), BB700 conjugated anti-CD19 (SJ25C1; BD), BUV496 conjugated anti-HLA-ABC (W6/32; BD), V450 conjugated anti-CD66b (G10F5; BD), BUV737 conjugated anti-CD86 (2331 (FUN-1); BD), BV510 conjugated anti-CD33 (WM53; BioLegend), BV480 conjugated anti-CD45 (HI30; BD), BV750 conjugated anti-CD34 (563; BD), APC conjugated anti-CD11c (Bu15; BioLegend)) were then added and incubated for 30 min at room temperature. Samples were washed two times with autoMACS running buffer (Miltenyi) and permeabilized using the Foxp3/transcription factor staining buffer set (eBioscience), followed by two more washes with the permeabilization buffer. The intracellular antibodies ((PE conjugated anti-TOX (TXRX10; Invitrogen), AF488 conjugated anti-TCF7 (S33-966; BD), PE-CF594 conjugated anti-STING (T3-680; BD), AF532 conjugated anti-CD3 (UCHT1; Invitrogen), PE-Cy5 conjugated anti-FoxP3 (PCH101; Invitrogen), AF700 conjugated anti-Ki67 (Ki-67; BioLegend)) were then added and incubated for 1 hour at room temperature, followed by two washes with permeabilization buffer and fixation in 1% paraformaldehyde. Antibody capture beads or amine-reactive beads (Thermo Fisher) were used for compensation. The stained cells were then analyzed using the Cytex Aurora spectral analyzer at the University of Washington's Department of Immunology Cell Analysis Facility. Spectral unmixing was performed using SpectroFlo software and the initial gating, selecting for single cells, lymphocytes, and live cells, was performed in FlowJo V.10 (FlowJo LLC; online supplemental figure 7). Further analysis was carried out in R.

scRNAseq sample preparation

Frozen tubes were thawed at 37°C, followed by the dropwise addition of complete media up to a total volume of 32 mL. Cells were then washed two times with PBS, counted and transferred to FACS tubes (Fisher Scientific). Live dead stain was then added (FVS780; BD Biosciences), followed by a blocking buffer to bring samples to 0.5% BSA, 5% TruStain FcX buffer (BioLegend), 100 nM dasatinib, and 50 µg salmon sperm. Samples were then incubated on ice for 10 min. DNA oligo-labeled HLA multimers were then added to patients with matched HLA types. Hashtag antibodies were added to identify sample origin in subsequent pooling steps. Fluorophore-labeled antibodies were then added followed by DNA oligo-labeled antibodies. Cells were then incubated on ice for 30 min and washed three times. Live cells were sorted

using an Aria II Cell sorter (BD Biosciences) into cold complete media, pooled, and immediately prepared for CITEseq (see below).

scRNAseq and scV(D)J-seq library preparation and sequencing

Single-cell suspensions (above) were loaded into the appropriate microfluidic chip (chip G; 10x Genomics) in a chromium controller (10x Genomics). Resulting cell suspensions then went through a library preparation process for scRNAseq along with paired scV(D)J-seq for TCR using the 5' transcriptome kit with feature barcoding (V.1.1; 10x Genomics) following the manufacturer's guidelines. The complementary DNA libraries were then sequenced using a NovaSeq instrument (Illumina) with 2×92 base pair paired-end reads aiming for an average of 20,000 reads per cell.

Beta TCR receptor profiling

Frozen PBMC or formalin-fixed paraffin-embedded (FFPE) tumor biopsy material (20 μm thick molecular curls) were used for DNA extraction using QIAamp DNA Blood Mini Kit or QIAamp DNA FFPE tissue kit respectively (Qiagen). Resulting samples were submitted to Adaptive Biotechnologies for TCRβ sequencing and normalization as previously described.³⁵

Immunohistochemistry

FFPE tissues were stained on a Leica BOND RX autostainer using the Akoya Opal Multiplex IHC assay (Akoya Biosciences, Menlo Park, CA) with the following changes: Additional high stringency washes were performed after the secondary antibody and Opal fluor applications using high-salt TBST (0.05M Tris, 0.3M NaCl, and 0.1% Tween-20, pH 7.2–7.6). TCT was used as the blocking buffer (0.05M Tris, 0.15M NaCl, 0.25% Casein, 0.1% Tween 20, pH 7.6±0.1). All primary antibodies were incubated for 1 hour at room temperature. Antibodies against the following targets were used for staining: CD56 (clone 123C3.D5; Bio SB), CD8 (clone C8/144B; DAKO), STING (clone SP338; Abcam) CD45 LCA (clone 2B11+PD7/26; DAKO), FoxP3 (clone 236A/E7; eBioscience), CD163 (clone ERP324; BioSB), CD68 (clone PG-M1; DAKO).

Slides were mounted with ProLong Gold and cured for 24 hours at room temperature in the dark before image acquisition at 20x magnification on the Akoya PhenoImager HT Automated Imaging System. Images were spectrally unmixed using Akoya inForm software.

HLA multimer preparation

HLA tetramers used for scRNAseq were created using HLA-I eamers (ImmunAware). BV421-labeled streptavidin (BioLegend) was used to prepare tetramers for flow cytometry experiments. PE or APC and DNA oligo nucleotide-labeled streptavidins (BioLegend) were used for scRNAseq experiments. Tetramers were titrated using samples of known positivity. Tetramers for six epitopes were created matching this patients HLA typing: Influenza A (HLA A*02:01 containing GILGFVFTL peptide),

EBV (HLA A*02:01 containing GLCTLVAML peptide), CMV (HLA A*02:01 containing NLVPMVATV peptide), and three MCPyV epitopes (HLA A*02:01 containing KLLEIANPC peptide; HLA A*11:01 containing RSGGFSFGK peptide and HLA A*37:01 containing KEWWRSGGF peptide).

Flow cytometry data analysis

Flow Cytometry Standard (FCS) files of live cells were loaded into a gating set object in R using flowWorkspace (V.4.6.0). Data from fluorescent markers was transformed using the bi-exponential function. Fluorescent minus one samples were used to draw minimum gates at the 99th percentile. Gates were adjusted upward as appropriate based on visual inspection. Uniform Manifold Approximation and Projection (UMAP) dimensionality reduction was performed using uwot (V.0.1.14). Clustering was performed using PhenoGraph (V.0.99.1). Visualization was performed using ggplot2 (V.3.4.0) or FlowJo (V.10.8.1).

scRNAseq data analysis

Data was analyzed as described elsewhere.³⁴ Briefly, the raw sequencing reads were aligned to the hg38 genome using Cell Ranger V.3.1. The filtered count matrices of transcripts and feature barcoding counts were then loaded into an R (V.4.1.2) SingleCellExperiment object for further analysis. The sample hash deconvolution was carried out using DropletUtils (V.1.14.2) and doublet detection and removal were done through scds (V.1.10.0) in conjunction with the doublets detected during hash deconvolution.

Low-quality cells with fewer than 800 transcript reads, fewer than 250 genes detected, or more than 10% of mitochondrial DNA were excluded from the analysis. The cells were size-normalized and log-transformed using scuttle (V.1.4.0). The cells from different runs were then integrated using the batchelor package (V.1.10.0). UMAP dimensionality reduction was performed with the integrated values. Clustering was done using the integrated transcript values and feature barcoding reads through the Walktrap algorithm on the nearest neighbor graph (scanr V.1.22.1). The number of clusters was varied by adjusting the number of nearest neighbors (k) during graph construction, followed by analysis using clustree (V.0.5.0).

Clusters were then labeled as the major cell lineages of CD4 T cells, CD8 T cells, B cells, myeloid cells, erythrocytes, NK cells, and cancer cells through the expression of key genes, including MS4A1, CD19, CD4, CD8A, CD3E, CD3D, GZMB, NCAM1, HLA-DRA, PTPRC, NKG7, and the MCPyV oncoproteins. The cluster labels were validated by investigating the portion of the cluster with productive TCR rearrangements. The cell lineages were isolated in silico and split into major lineages, and dimensionality reduction and clustering were reperformed as described above. Clonotypes (TCRs) were identified as MCPyV-specific if the clonotype bound more than a mean

of 40CD8 antibodies, less than a mean of 40CD4 antibodies and more than a mean of 244 multimer molecules. Of note, six clonotypes bound sufficient levels of CD8 and multimer but were excluded due to high levels of CD4 and were excluded from further analysis due to concerns for non-specific binding.

The cells were scored for the expression of HLA and interferon gene sets using the UCell (V.1.99.1) package. Plotting was performed using scater (V.1.22.0), Seurat (V.4.3.0), or ggplot2 (V.3.4.0).

Gene sets

Genes associated with antigen presentation were taken from the antigen presentation and processing data set from Biocarta.³⁶ HLA genes B, C, E and F not originally included in the set were added for completeness. Genes associated with interferon alpha or gamma signatures were taken from the respective hallmark gene sets.²¹

ADU-S100 stimulation

To assess MCC cell lines response to STING agonism, the virus-positive cell lines WaGa, MKL1, MKL2 and MS-1 as well as a human monocytic cell line (THP1; positive control) were treated with ADU-S100. 100,000 cells were plated in 0.25 mL of media. ADU-S100 (MedChemExpress) was added to bring final concentrations to 100, 20, 4, 0.8, or 0.016 micromolar. The concentration of interferon beta was measured in media 48 hours later via ELISA (R&D Systems). All samples run in triplicate.

Western blot

WaGa, MKL1, MKL2, MS-1 and THP-1 cells were seeded in T75 flasks and maintained at 37°C in a humidified incubator with 5% CO₂. Cells were pelleted and lysed in ice-cold buffer containing 150 mM NaCl, 1.0% IGEPAL CA-630, 0.5% sodium deoxycholate, 0.1% SDS, 50 mM Tris (pH 8.0) and protease/phosphatase inhibitor cocktail (1:100; Cell Signaling Technology, USA). Soluble fractions from prepared cell lysates were collected after centrifugation at 13,000 rpm for 10 min at 4°C. Next, normalized cell lysates (quantified using Bradford assay) were separated by 10% Sodium dodecyl sulfate-polyacrylamide gel electrophoresis (SDS-PAGE), transferred onto polyvinylidene fluoride (PVDF) membranes, and immunoblotted with STING (1:1,000; Cell Signaling Technology, USA) / β -actin (1:10,000; Sigma-Aldrich, USA) primary antibody and anti-rabbit (1:2,500; Cell Signaling Technology, USA) / anti-mouse (1:2,500; Cell Signaling Technology, USA) horseradish peroxidase-conjugated secondary antibody respectively. Blotted proteins were visualized on x-ray films incubated with a high-sensitivity enhanced chemiluminescence (ECL) reagent (Sigma-Aldrich, USA).

Statistics

T-tests were used to compare differences between two groups unless otherwise noted. When comparing more than two groups, the non-parametric Kruskal-Wallis test or one-way analysis of variance was used as indicated. Multiple hypothesis testing was done with the Bonferroni

method unless noted differently. Fisher's exact test was used to evaluate differences between two categorical variables. Differentially abundant T cell clones (beta-TCRseq) were identified using a two-sided beta-binomial test with an alpha value of 0.01 as calculated per the Adaptive Analyzer platform. All other statistical analysis was carried out using R V.4.1+ or GraphPad Prism V.9.5.

Author affiliations

¹Department of Dermatology, University of Washington School of Medicine, Seattle, Washington, USA

²Fred Hutchinson Cancer Center, Seattle, Washington, USA

³Department of Radiation Oncology, University of Washington, Seattle, Washington, USA

⁴Division of Medical Oncology, University of Washington School of Medicine, Seattle, Washington, USA

⁵Department of Laboratory Medicine and Pathology, University of Washington School of Medicine, Seattle, Washington, USA

⁶Department of Medicine, University of Washington School of Medicine, Seattle, Washington, USA

Acknowledgements Figure schematics created using BioRender.com. This research was supported by the Experimental Histopathology shared resource of the Fred Hutch/University of Washington Cancer Consortium (P30 CA015704).

Contributors TP, PN, and SB designed the experiments and are guarantors. SB treated the subject patient. RK prepared specimens. KS and BWS performed multiplexed immunohistochemistry staining. RB performed western blots. TP performed all other experiments. TP and SJ analyzed all data. SJ, PHG, ST-C, LT, RK, CC, and DK provided scientific guidance. TP wrote the original manuscript. All authors reviewed the manuscript and approved its publication.

Funding Supported by the National Cancer Institute (NCI) Grants No. P01 CA225517 (DK, PN, SB), F30 CA254168 (TP), T32 CA080416 (SJ) and the National Institutes of Health/NCI Cancer Center Support Grant in Seattle Grant No. P30 CA015704. RB reports support from ASPIRE II award (22-003-AS). Scientific computing infrastructure at Fred Hutchinson Cancer Center was funded by US NIH ORIP grant S10 OD028685. We would like to acknowledge support from the Merkel cell carcinoma patient gift fund at the University of Washington and the Kelsey Dickson Team Science Courage Research Award: Advancing New Therapies for Merkel Cell Carcinoma (MCC).

Competing interests PN reports personal fees from Pfizer, Bristol Myers Squibb, EMD Serono, Rain Therapeutics, Almirall, and Instill Bio. In addition, PN and DK have pending patents for "Merkel cell polyomavirus T antigen-specific TCRs and uses thereof" and "Novel epitopes as T cell targets in Merkel Cell Carcinoma (MCC)". CC has a pending patent "Merkel cell polyomavirus T antigen-specific TCRs and uses thereof". LT reports research grant funding (to institution) from Seagen and Merck. SB has received consulting or advisory role fees and honoraria from Bristol Myers Squibb, Sanofi/Regeneron, and Incyte; and has received research funding from Bristol Myers Squibb, Merck, EMD Serono, Excure, Incyte, Checkmate Pharmaceuticals, 4SC, Seven and Eight Pharmaceuticals, Amphivena Therapeutics, TriSalus Life Sciences, Novartis and Agenus. DK reports research funding from Sanofi Pasteur. DK has received consulting or advisory fees from Curevo Vaccine and MaxHealth LLC Pasteur. KS has received consulting or advisory role fees from Sensei Biotherapeutics.

Patient consent for publication Not applicable.

Ethics approval This study involves human participants and was approved by Fred Hutch Cancer Center IRB#6585. Participants gave informed consent to participate in the study before taking part.

Provenance and peer review Not commissioned; externally peer reviewed.

Data availability statement Data are available in a public, open access repository. Data are available upon reasonable request. Single-cell RNA sequencing and single-cell T-cell receptor sequencing data is available on the Gene Expression Omnibus under ascension number GSE227709.³⁷ Flow cytometry data available upon reasonable request.

Supplemental material This content has been supplied by the author(s). It has not been vetted by BMJ Publishing Group Limited (BMJ) and may not have been peer-reviewed. Any opinions or recommendations discussed are solely those

of the author(s) and are not endorsed by BMJ. BMJ disclaims all liability and responsibility arising from any reliance placed on the content. Where the content includes any translated material, BMJ does not warrant the accuracy and reliability of the translations (including but not limited to local regulations, clinical guidelines, terminology, drug names and drug dosages), and is not responsible for any error and/or omissions arising from translation and adaptation or otherwise.

Open access This is an open access article distributed in accordance with the Creative Commons Attribution Non Commercial (CC BY-NC 4.0) license, which permits others to distribute, remix, adapt, build upon this work non-commercially, and license their derivative works on different terms, provided the original work is properly cited, appropriate credit is given, any changes made indicated, and the use is non-commercial. See <http://creativecommons.org/licenses/by-nc/4.0/>.

ORCID iDs

Thomas Pulliam <http://orcid.org/0000-0003-3511-6348>
 Peter H Goff <http://orcid.org/0000-0002-3488-4997>
 Kimberly Smythe <http://orcid.org/0000-0002-2329-8298>
 Lisa Tachiki <http://orcid.org/0000-0001-8057-8029>
 Candice Church <http://orcid.org/0000-0003-1582-8292>
 David M Koelle <http://orcid.org/0000-0003-1255-9023>
 Paul Nghiem <http://orcid.org/0000-0003-2784-963X>
 Shailender Bhatia <http://orcid.org/0000-0002-3816-2238>

REFERENCES

- Samson N, Ablasser A. The cGAS-STING pathway and cancer. *Nat Cancer* 2022;3:1452–63.
- Francica BJ, Ghasemzadeh A, Desbien AL, et al. TNF α and Radioresistant Stromal Cells Are Essential for Therapeutic Efficacy of Cyclic Dinucleotide STING Agonists in Nonimmunogenic Tumors. *Cancer Immunol Res* 2018;6:422–33.
- Corrales L, Glickman LH, McWhirter SM, et al. Direct Activation of STING in the Tumor Microenvironment Leads to Potent and Systemic Tumor Regression and Immunity. *Cell Rep* 2015;11:1018–30.
- Downey CM, Aghaei M, Schwendener RA, et al. DMXAA causes tumor site-specific vascular disruption in murine non-small cell lung cancer, and like the endogenous non-canonical cyclic dinucleotide STING agonist, 2'3'-cGAMP, induces M2 macrophage repolarization. *PLoS ONE* 2014;9:e99988.
- Ohkuri T, Ghosh A, Kosaka A, et al. STING contributes to antitumor immunity via triggering type I IFN signals in the tumor microenvironment. *Cancer Immunol Res* 2014;2:1199–208.
- Deng L, Liang H, Xu M, et al. STING-Dependent Cytosolic DNA Sensing Promotes Radiation-Induced Type I Interferon-Dependent Antitumor Immunity in Immunogenic Tumors. *Immunity* 2014;41:843–52.
- Harding SM, Benci JL, Irianto J, et al. Mitotic progression following DNA damage enables pattern recognition within micronuclei. *Nature New Biol* 2017;548:466–70.
- Woo SR, Fuertes MB, Corrales L, et al. STING-dependent cytosolic DNA sensing mediates innate immune recognition of immunogenic tumors. *Immunity* 2014;41:830–42.
- Haddox CL, Nathenson MJ, Mazzola E, et al. Phase II Study of Eribulin plus Pembrolizumab in Metastatic Soft-tissue Sarcomas: clinical Outcomes and Biological Correlates. *Clin Cancer Res* 2024;30:1281–92.
- Meric-Bernstam F, Sweis RF, Kasper S, et al. Combination of the STING Agonist MIW815 (ADU-S100) and PD-1 Inhibitor Spaltalizumab in Advanced/Metastatic Solid Tumors or Lymphomas: an Open-Label, Multicenter, Phase Ib Study. *Clin Cancer Res* 2023;29:110–21.
- Meric-Bernstam F, Sweis RF, Hodi FS, et al. Phase I Dose-Escalation Trial of MIW815 (ADU-S100), an Intratumoral STING Agonist, in Patients with Advanced/Metastatic Solid Tumors or Lymphomas. *Clin Cancer Res* 2022;28:677–88.
- Luke JJ, Piha-Paul SA, Medina T, et al. Phase I Study of SYN1891, an Engineered E. Coli Nissle Strain Expressing STING Agonist, with and without Atezolizumab in Advanced Malignancies. *Clin Cancer Res* 2023;29:2435–44.
- Marcus A, Mao AJ, Lensink-Vasan M, et al. Tumor-Derived cGAMP Triggers a STING-Mediated Interferon Response in Non-tumor Cells to Activate the NK Cell Response. *Immunity* 2018;49:754–63.
- Sivick KE, Desbien AL, Glickman LH, et al. Magnitude of Therapeutic STING Activation Determines CD8⁺ T Cell-Mediated Anti-tumor Immunity. *Cell Rep* 2018;25:3074–85.
- Harms PW, Harms KL, Moore PS, et al. The biology and treatment of Merkel cell carcinoma: current understanding and research priorities. *Nat Rev Clin Oncol* 2018;15:763–76.
- Paulson KG, Iyer JG, Tegeder AR, et al. Transcriptome-wide studies of merkel cell carcinoma and validation of intratumoral CD8⁺ lymphocyte invasion as an independent predictor of survival. *J Clin Oncol* 2011;29:1539–46.
- Nghiem P, Bhatia S, Lipson EJ, et al. Three-year survival, correlates and salvage therapies in patients receiving first-line pembrolizumab for advanced Merkel cell carcinoma. *J Immunother Cancer* 2021;9:e002478.
- D'Angelo SP, Lebbé C, Mortier L, et al. First-line avelumab in a cohort of 116 patients with metastatic Merkel cell carcinoma (JAVELIN Merkel 200): primary and biomarker analyses of a phase II study. *J Immunother Cancer* 2021;9:e002646.
- Bhatia S, Nghiem P, Veeranki SP, et al. Real-world clinical outcomes with avelumab in patients with Merkel cell carcinoma treated in the USA: a multicenter chart review study. *J Immunother Cancer* 2022;10:e004904.
- Topalian SL, Bhatia S, Amin A, et al. Neoadjuvant Nivolumab for Patients With Resectable Merkel Cell Carcinoma in the CheckMate 358 Trial. *J Clin Oncol* 2020;38:2476–87.
- Liberzon A, Birger C, Thorvaldsdóttir H, et al. The Molecular Signatures Database (MSigDB) hallmark gene set collection. *Cell Syst* 2015;1:417–25.
- Simoni Y, Becht E, Fehlings M, et al. Bystander CD8⁺ T cells are abundant and phenotypically distinct in human tumour infiltrates. *Nat New Biol* 2018;557:575–9.
- Liu W, Kim GB, Krump NA, et al. Selective reactivation of STING signaling to target Merkel cell carcinoma. *Proc Natl Acad Sci U S A* 2020;117:13730–9.
- Jing W, McAllister D, Vonderhaar EP, et al. STING agonist inflames the pancreatic cancer immune microenvironment and reduces tumor burden in mouse models. *J Immunother Cancer* 2019;7:115.
- Ramanjulu JM, Pesiridis GS, Yang J, et al. Design of amidobenzimidazole STING receptor agonists with systemic activity. *Nat New Biol* 2018;564:439–43.
- Lee PC, Klaefer S, Le PM, et al. Reversal of viral and epigenetic HLA class I repression in Merkel cell carcinoma. *J Clin Invest* 2022;132:e151666.
- Ritter C, Fan K, Paschen A, et al. Epigenetic priming restores the HLA class-I antigen processing machinery expression in Merkel cell carcinoma. *Sci Rep* 2017;7:2290.
- Paulson KG, Voillet V, McAfee MS, et al. Acquired cancer resistance to combination immunotherapy from transcriptional loss of class I HLA. *Nat Commun* 2018;9:3868.
- Paulson KG, Tegeder A, Willmes C, et al. Downregulation of MHC-I expression is prevalent but reversible in Merkel cell carcinoma. *Cancer Immunol Res* 2014;2:1071–9.
- Lau L, Gray EE, Brunette RL, et al. DNA tumor virus oncogenes antagonize the cGAS-STING DNA-sensing pathway. *Science* 2015;350:568–71.
- Feng H, Shuda M, Chang Y, et al. Clonal integration of a polyomavirus in human Merkel cell carcinoma. *Science* 2008;319:1096–100.
- Walsh NM, Fleming KE, Hanly JG, et al. A morphological and immunophenotypic map of the immune response in Merkel cell carcinoma. *Hum Pathol* 2016;52:190–6.
- Longino NV, Yang J, Iyer JG, et al. Human CD4⁺ T Cells Specific for Merkel Cell Polyomavirus Localize to Merkel Cell Carcinomas and Target a Required Oncogenic Domain. *Cancer Immunol Res* 2019;7:1727–39.
- Pulliam T, Jani S, Jing L, et al. Circulating cancer-specific CD8 T cell frequency is associated with response to PD-1 blockade in Merkel cell carcinoma. *Cell Rep Med* 2024;5:101412.
- Robins HS, Campregher PV, Srivastava SK, et al. Comprehensive assessment of T-cell receptor beta-chain diversity in alphabeta T cells. *Blood* 2009;114:4099–107.
- Rouillard AD, Gundersen GW, Fernandez NF, et al. The harmonizome: a collection of processed datasets gathered to serve and mine knowledge about genes and proteins. *Database (Oxf)* 2016;2016:baw100.
- Pulliam T, Jani S, Nghiem P, et al. Sting agonist leads to durable clinical response in an anti-pd-1 refractory patient: tumor antigen-specific, single cell level biomarker analyses. gene expression omnibus. 2023. Available: <https://www.ncbi.nlm.nih.gov/geo/query/acc.cgi?acc=GSE227709>